Magnetic Hair and Reconnection in Black Hole Magnetospheres

Ashley Bransgrove[1,*], Bart Ripperda[2,3] and Alexander Philippov[2]

[1]*Physics Department and Columbia Astrophysics Laboratory, Columbia University,*
538 West 120th Street, New York, New York 10027, USA
[2]*Center for Computational Astrophysics, Flatiron Institute, 162 Fifth Avenue, New York, New York 10010, USA*
[3]*Department of Astrophysical Sciences, Peyton Hall, Princeton University, Princeton, New Jersey 08544, USA*

The no-hair theorem of general relativity states that isolated black holes are characterized by three parameters: mass, spin, and charge. In this Letter we consider Kerr black holes endowed with highly magnetized plasma-filled magnetospheres. Using general relativistic kinetic plasma and resistive magnetohydrodynamics simulations, we show that a dipole magnetic field on the event horizon opens into a split monopole and reconnects in a plasmoid-unstable current sheet. The no-hair theorem is satisfied, in the sense that all components of the stress-energy tensor decay exponentially in time. We measure the decay time of magnetic flux on the event horizon for plasmoid-dominated reconnection in collisionless and collisional plasma. The reconnecting magnetosphere should be a powerful source of hard x-ray emission when the magnetic field is strong.

Black holes (BHs) formed by the collapse of a magnetized progenitor are born with magnetic fields penetrating the event horizon. There are several possible scenarios, such as the spin-down of a rotationally supported hypermassive neutron star (NS) [1], or gravitational collapse induced by the accretion of dark matter onto the NS core [2]. BHs can also acquire magnetic flux later in life by merging with a magnetized NS [3], or in accretion flows. The fate of the magnetic flux (hair) on the event horizon should be in accordance with the no-hair theorem of general relativity.

The original no-hair conjecture [4] states that all stationary, asymptotically flat BH spacetimes should be completely described by the mass, angular momentum, and electric charge. It was later proved formally that any field with zero rest mass and arbitrary integer spin is radiated away on a light-crossing timescale [5]. In particular, the multipole component l of a magnetic field in vacuum decays as $t^{-(2l+2)}$. However, magnetized BHs are unlikely to exist in vacuum. If a BH is formed by the collapse of a magnetized star, plasma will inevitably exist in the magnetosphere around the newly formed event horizon. Furthermore, BHs can generate a self-regulated plasma supply through electron-positron discharges near the event horizon [6–8]. The discharges can fill the magnetosphere with plasma in a light-crossing time.

The presence of highly conducting plasma, and thus a nonzero stress-energy tensor of matter, dramatically changes the vacuum dynamics assumed in the classical no-hair theorem. Essentially, in the limit of vanishing resistivity a topological constraint is imposed which prevents the magnetic field from sliding off the event horizon [9]. The only

way for the BH to lose its magnetic field is for the field to change its topology (reconnect). Fast magnetic reconnection occurs through the tearing instability [10]. A chain of plasmoids (magnetic loops containing plasma) forms along the reconnection layer which are ejected at relativistic velocities. For highly magnetized collisionless plasma (as expected in a BH magnetosphere), the reconnection rate $v_{\rm rec} \sim 0.1c$ is independent of the magnetization [11–13]. The lifetime of the magnetic flux on the event horizon should be determined in part by this universal reconnection rate.

Previous work in an ideal fluid approximation correctly established the qualitative evolution of a dipole magnetic field on the event horizon opening into a split monopole [9]. However, it neglected collisionless physics, and was performed at low numerical resolution such that the reconnection was not in the high Lundquist number regime [9,14]. This lead to the conclusion of an extremely long lifetime of the magnetic flux on the event horizon, dictated by the resistive timescale of the plasma [9]. In this Letter we describe for the first time GRPIC (general-relativistic particle-in-cell) and GRRMHD (general-relativistic resistive magnetohydrodynamics) simulations which are converged and produce the correct reconnection physics.

The system is solved numerically in Kerr spacetime. Kerr-schild coordinates (t, r, θ, ϕ) are used so that all quantities are regular at the event horizon. The dimensionless BH spin is set to $a = 0.99$ to maximize the ergosphere volume. We define "fiducial observers" (FIDOs), whose worldlines are normal to spatial hypersurfaces. We assume that the neutron star was already surrounded by plasma, and that it collapsed into a BH before the simulation begins. This setup is sufficient to test the no-hair theorem because

when plasma is present, the magnetic field cannot escape before the event horizon has formed [9]. The initial condition for all simulations is a magnetic dipole described by the vector potential $A_\phi = B_0 \sin^2\theta/r$, where B_0 is the dimensionless magnetic field strength at the horizon as measured by the FIDO. The magnetic field components are obtained from $B^i = \epsilon^{ijk}\partial_j A_k/\sqrt{\gamma}$, where $\sqrt{\gamma}$ is the spatial metric determinant. In vacuum nonzero $\nabla \times (\alpha \boldsymbol{B})$ is quickly radiated away or swallowed by the BH (α is the lapse). However, when plasma is present nonzero $\nabla \times (\alpha \boldsymbol{B})$ drives currents which slow down the balding process.

The kinetic plasma simulations are performed using the general-relativistic particle-in-cell (PIC) code Zeltron [7]. We solve the equations of motion for pair plasma particles, together with Maxwell's equations for electromagnetic fields. All lengths are given in units of $r_g = GM/c^2$ with M the BH mass, and times in units of r_g/c. The particles have mass m, and charge $\pm e$. The GRPIC simulations begin with vacuum, and plasma particles are injected with density proportional to the local parallel electric field as a proxy for the electron-positron discharge (see [7] for details of the injection scheme).

We set the dimensionless magnetic field strength at the event horizon $B_0 = r_g/r_L$, with r_L the Larmor radius. For the gravitational collapse of a neutron star it implies $B_0 \sim 10^{14}(M/M_\odot)(B/10^{12} \text{ G})$. In this work we scale it down, and consider $B_0 \sim 10^4, 3 \times 10^4, 10^5$ (Table I). We show that our results are independent of B_0, as long as the plasma is highly magnetized. The characteristic minimum plasma density required to support the rotating magnetosphere is the Goldreich-Julian number density [15], $n_0 = \Omega_H B_0/(2\pi c e)$, where $\Omega_H = a c r_g/[r_H^2 + (r_g a)^2]$ is the angular velocity of the event horizon radius $r_H = r_g(1 + \sqrt{1-a^2})$. It implies the characteristic magnetization $\sigma_0 = B_0^2/(4\pi n_0 m c^2) = (1/2)(\omega_B/\Omega_H) = (1/4)(\omega_p/\Omega_H)^2 \gg 1$, where $\omega_p = (4\pi n_0 e^2/m)^{1/2}$ is the plasma frequency and $\omega_B = c/r_L$ the Larmor frequency.

TABLE I. Summary of the simulation parameters. For all GRRMHD runs the diffusivity is $\eta = 10^{-5}$. For MHD runs $N_r \times N_\theta \times N_\phi$ refers to the effective resolution. Runs with $N_\phi = 1$ are axisymmetric, while those with $N_\phi > 1$ refer to 3D simulations. All models have spin $a = 0.99$ except VAC0, which has $a = 0$.

Model	r_L	λ_p	$N_r \times N_\theta \times N_\phi$
VAC0	$\cdots$	$\cdots$	$9600 \times 8016 \times 1$
VAC1	$\cdots$	$\cdots$	$9600 \times 8016 \times 1$
GRPIC1	1×10^{-5}	3×10^{-3}	$2880 \times 2160 \times 1$
GRPIC2	3×10^{-5}	6×10^{-3}	$2880 \times 2160 \times 1$
GRPIC3	1×10^{-4}	1×10^{-2}	$2880 \times 2160 \times 1$
GRRMHD1	$\cdots$	$\cdots$	$6144 \times 3072 \times 1$
GRRMHD2	$\cdots$	$\cdots$	$3072 \times 1536 \times 1536$

We have preserved the astrophysically relevant hierarchy of scales $r_L \ll \lambda_p \ll r_g$, and $\Omega_H \ll \omega_p \ll \omega_B$, where $\lambda_p = c/\omega_p$ is the plasma skin depth.

The computational domain of the axisymmetric GRPIC simulations covers $0.99 \leq r \leq 75$, and $0 \leq \theta \leq \pi$. Simulations for each of the (three) magnetic field strengths were performed at two resolutions to check for numerical convergence (a total of six kinetic plasma simulations): (i) $N_r \times N_\theta = 1440 \times 1080$, and (ii) $N_r \times N_\theta = 2880 \times 2160$. The grid is uniformly spaced in $\log r$ and $\cos\theta$, so that the resolution is concentrated near the BH horizon, and the equator. We check that the plasma skin depth is well resolved *a posteriori*, since the plasma density is determined self-consistently. Electromagnetic fields are damped and particles are absorbed at the outer boundary in order to mimic an outflow boundary condition. For $r \leq r_H$ all characteristics are inward, and causality prevents waves and plasma from escaping. Therefore, the equations are solved without modification at the event horizon, and no boundary condition is imposed there.

The GRRMHD simulations are performed using the Black Hole Accretion Code [16–18]. A minimum density is set throughout the domain such that the magnetization $\sigma \gg 1$, and the plasma is nearly force-free. We set a constant and uniform diffusivity $\eta = 10^{-5}$, so that the Lundquist number $S = v_A L/\eta \approx \eta^{-1} = 10^5$ is above the plasmoid instability limit $S > 10^4$ [10], where $v_A \approx c$ is the Alfvén speed and $L \approx r_e - r_g \approx 1$ is the characteristic length of the current sheet inside the ergosphere.

The computational domain of the GRRMHD simulations covers $0.99 \leq r \leq 200$, $0 \leq \theta \leq \pi$, and $0 \leq \phi \leq 2\pi$. By adding AMR, we increase the resolution at the current sheet to assure convergence. The base grid, and additional AMR blocks are uniformly spaced in $\log r$, and ϕ, while the θ grid is concentrated near the equator.

The evolution of all simulations is qualitatively similar. In GRPIC simulations, strong electric fields induced by spacetime rotation near the event horizon trigger particle injection which rapidly fills the magnetosphere with plasma up to a density $n \sim \mathcal{M} n_0$, where $\mathcal{M} \sim$ few is the multiplicity, while GRRMHD simulations begin with a static low-density plasma throughout the domain. In the ergosphere plasma is dragged into corotation with the BH, bending field lines in the ϕ direction and inflating the poloidal magnetic field. As field lines extend in the radial direction, flux on the horizon moves toward the equator, and some loops which close inside the ergosphere are pushed into the BH. After $t \approx 40 \ r_g/c$, the dipole has opened into a split monopole with $\boldsymbol{\Omega} \cdot \boldsymbol{B}_p > 0$ in both hemispheres, where $\boldsymbol{\Omega}$ is the angular velocity vector of the BH and $\boldsymbol{B}_p$ is the poloidal magnetic field. The field lines rotate rigidly with angular velocity $\Omega_F = \Omega_H/2$, in agreement with force-free solutions [6]. The toroidal magnetic field H_ϕ has opposite sign to B^r in each hemisphere (Fig. 1, right) indicating swept-back field lines, where
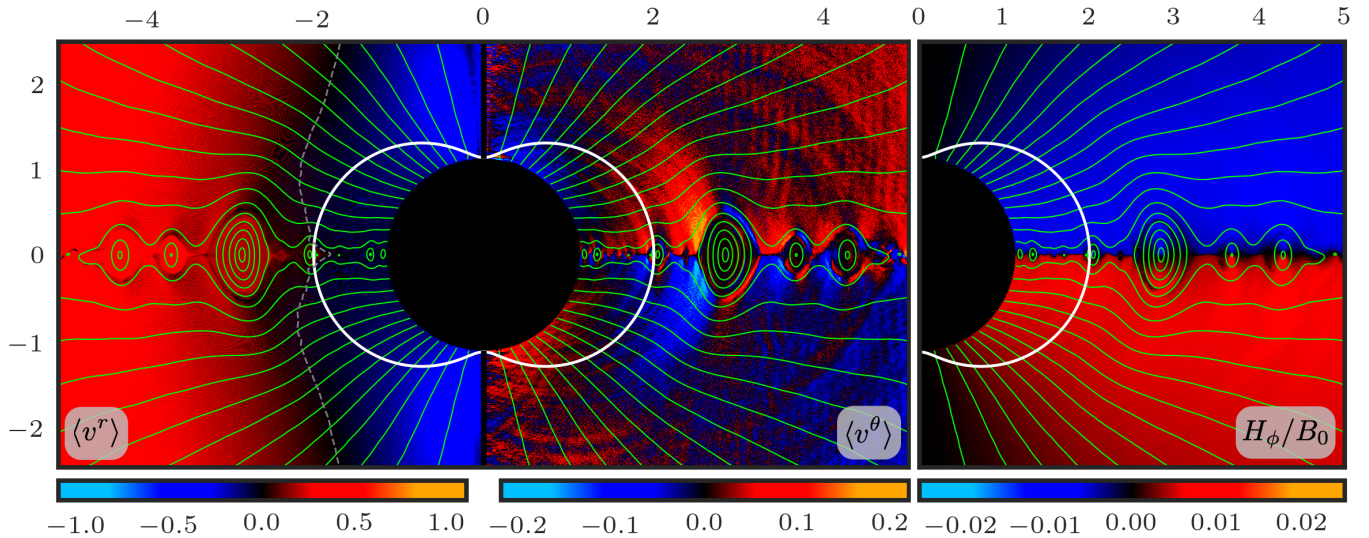
FIG. 1.   Reconnecting magnetosphere in the FIDO frame (GRPIC1) at $t = 100 \; r_g/c$. Green curves show poloidal magnetic flux surfaces, and white curves show the boundary of the ergosphere. The black circle is the interior of the BH event horizon. Left: color shows radial and θ components of the bulk plasma three-velocity in the orthonormal tetrad basis. The grey dashed curve indicates the stagnation surface defined by $\langle v^r \rangle = 0$. Right: azimuthal component of the auxiliary field $\boldsymbol{H}$.

$\boldsymbol{H} = \alpha \boldsymbol{B} - \boldsymbol{\beta} \times \boldsymbol{D}$, $\boldsymbol{\beta}$ is the shift, and $\boldsymbol{D}$ the electric field. A well-defined MHD stagnation surface is established, separating regions of inflow $\langle v^r \rangle < 0$, and outflow $\langle v^r \rangle > 0$ (Fig. 1, dashed grey curve). Here $\langle \cdots \rangle$ indicates averaging over the particles in a single grid cell.

Magnetic reconnection is first triggered near the stagnation surface in both GRPIC and GRRMHD, and rapidly spreads along the entire current sheet. The onset of reconnection occurs later in GRRMHD simulations $t \sim 70 \; r_g/c$, compared to GRPIC simulations $t \sim 30 \; r_g/c$. However, once the current sheet is sufficiently thin the tearing instability develops and a chain of self-similar plasmoids forms. Generally plasmoids born inside the stagnation surface move slowly ($v < 0.1c$) toward the event horizon and fall into the BH, while those born outside are ejected from the magnetosphere and accelerate to relativistic velocities ($v \approx c$). Therefore, we identify the stagnation surface at the equator as a main site of field-line "pinching," and a primary X point in the global magnetosphere. Occasionally plasmoids born inside the stagnation surface have sufficient kinetic energy to escape.

We analyzed the reconnection rate for all simulations by measuring the inflow velocity of flux into the current sheet. The analysis is performed by transforming the electric and magnetic field components into the locally Minkowski reference frame of the FIDO. The inflow velocity is then calculated using the component of $\boldsymbol{E} \times \boldsymbol{B}$ in the direction perpendicular to the current sheet, and avoiding plasmoids. We confirm $\sigma \gg 1$ in the upstream plasma, so that $v_A/c = [\sigma/(\sigma + 1)]^{1/2} \approx 1$, and the reconnection is in the relativistic regime. All components of the magnetic field change sign at the current sheet, indicating zero guide-field reconnection.

The measured reconnection rate in the GRPIC simulations $v_{\text{rec}} \approx 0.1c$ is consistent with studies of magnetic reconnection in relativistic collisionless plasmas [11–13]. For the GRRMHD simulations the high Lundquist number $S \approx 10^5 \gg 10^4$ ensures that the reconnection occurs deep in the plasmoid dominated regime [19]. The reconnection rate in resistive MHD at high Lundquist number is $v_{\text{rec}} \approx 0.01v_A$ [10], which is confirmed by our measured $v_{\text{rec}} \approx 0.01c$–$0.02c$ and is consistent with other studies in relativistic MHD [20] where the reconnection dynamics is modified by $v_A \to c$. In GRPIC simulations the plasmoids grow at a rate $\sim 0.1c$, until they are ejected and the growth is suppressed as they reach relativistic velocities. Thus the plasmoids are on average smaller in GRRMHD simulations (Fig. 2), where the growth rate $\sim 0.01c$ is smaller.

Reconnection in collisionless pair plasma occurs due to kinetic effects resulting from the divergence of the anisotropic electron pressure tensor, which plays the role of an effective nonuniform diffusivity [21]. Therefore, the difference in reconnection rates between the two formalisms can be attributed to the use of a uniform diffusivity in GRRMHD simulations as a proxy for kinetic effects, representing the simplest model of reconnection and plasmoid formation, while in GRPIC simulations the dissipation at the current sheet is determined from first principles.

The reconnection is collisionless when the plasma skin depth λ_p is larger than the elementary current sheet width in the resistive-MHD chain $w \sim 100\eta/v_A \sim 100\eta/c$ [10,22], where η is the diffusivity due to Coulomb collisions of pairs. Since our simulations do not include the detailed pair production and collision physics, we estimate analytically when this condition is satisfied [23]. The temperature of the
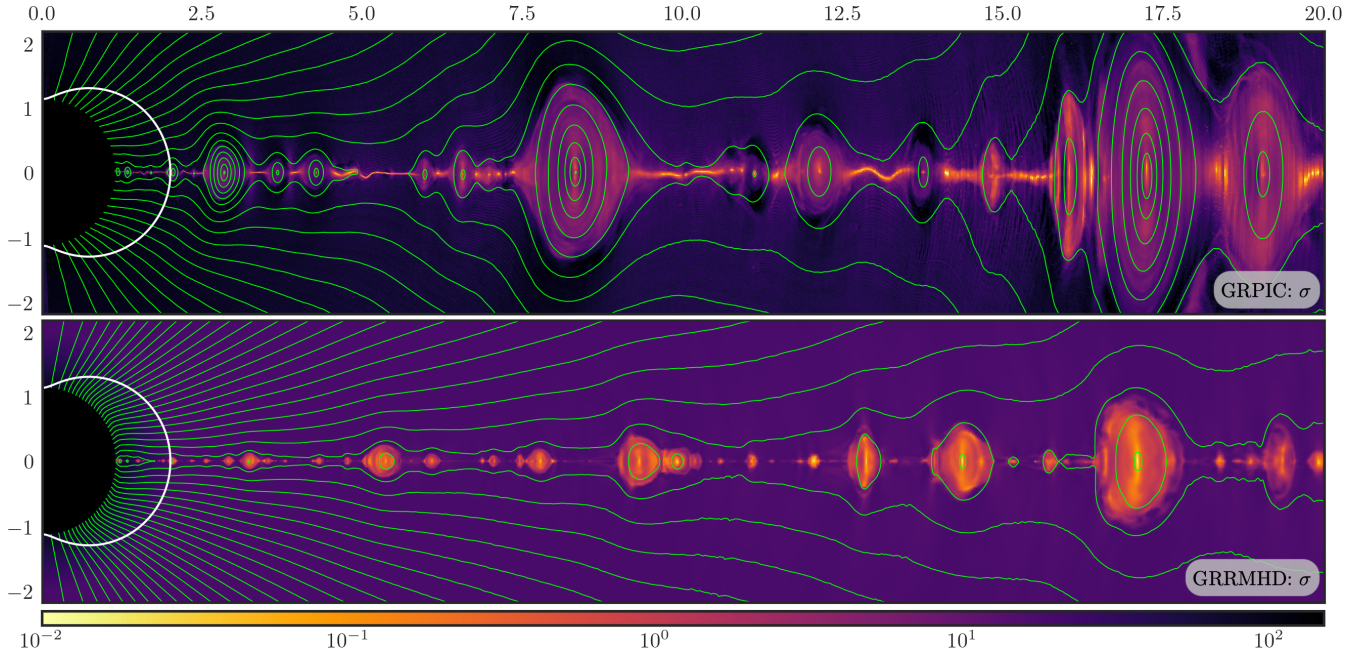
FIG. 2. Different realizations of the reconnecting magnetosphere in the FIDO frame. Color shows the cold plasma magnetization σ. Top: GRPIC1 at $t = 100 \, r_g/c$, $\sigma = B^2/(4\pi mnc^2)$. Bottom: GRRMHD1 at $t = 311 \, r_g/c$, $\sigma = B^2/(4\pi\rho c^2)$. The GRPIC simulation (top) displays larger plasmoids than GRRMHD (bottom) due to the faster reconnection rate of collisionless plasma.

reconnection layer is estimated by assuming the combined pressure of radiation and pairs is comparable to $B^2/(8\pi)$. The density of pairs is then given by the annihilation balance. We find that the reconnection is evidently collisionless when $B \ll 10^{12}$ G. However, if the magnetic field is very strong $B \gtrsim 10^{12}$ G, or pair production is very efficient, the separation between the two regimes is less clear, and a self-consistent calculation is required to determine the reconnection rate. However, even in this intermediate case, the GRRMHD simulations described in this work with uniform η provide a lower limit on the reconnection rate.

The magnetic flux on the event horizon Φ decays quasiexponentially with time (Fig. 3). In GRPIC simulations the flux decays with characteristic timescale $\tau \approx 100$ r_g/c, and in GRRMHD simulations $\tau \approx 500 \, r_g/c$ (Fig. 3). The difference in timescales can be attributed to different reconnection rates in these formalisms, which differ by a factor ~ 5. Since B and $n \propto B$ decay exponentially, all components of the stress-energy tensor become vanishingly small at late times and the no-hair theorem is satisfied. We calculate the charge of the BH at the end of the GRPIC simulation as $Q = (1/4\pi) \int D^r \sqrt{\gamma} d\theta d\phi$ at $r = r_H$ and find that $Q = 0$, so the final state is a Kerr BH.

The decay timescale converges with decreasing r_L/r_H in the GRPIC simulations (Fig. 3), indicating the correct asymptotic behavior with a sufficient separation of scales. Therefore, the measured decay timescale is independent of B, as long as the plasma is highly magnetized, $\sigma \gg 1$,

and finite Larmor radius corrections are negligible, $r_L/r_g \ll 1$.

The evolution of Φ is estimated analytically using Faraday's law, and assuming a constant reconnection rate on the equator at the stagnation surface [23,27]. In this toy model Φ decays exponentially on a timescale $\tau \approx 3r_g/\langle v^\theta \rangle$, with $\langle v^\theta \rangle$ the θ component of the plasma three-velocity in the orthonormal tetrad basis (Fig. 1). For example, in GRPIC1 the measured $\langle v^\theta \rangle \approx 0.02$–$0.04c$ at the current sheet implies $\tau \sim 100 \, r_g/c$, consistent with Fig. 3. The local
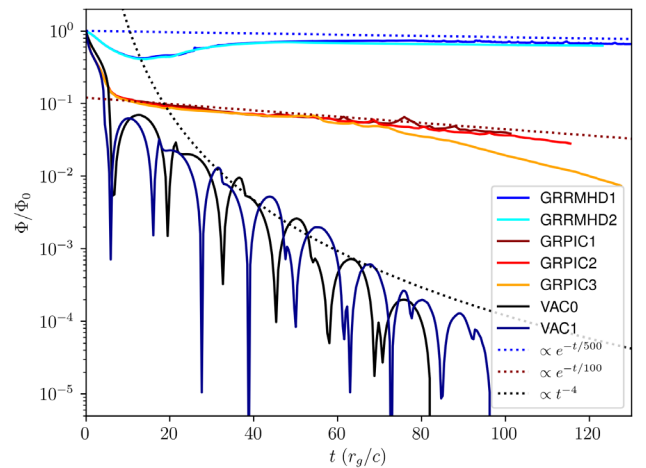

FIG. 3. Flux on the event horizon vs time for vacuum (power law decay), collisional MHD plasma (exponential decay), and collisionless plasma (faster exponential decay).
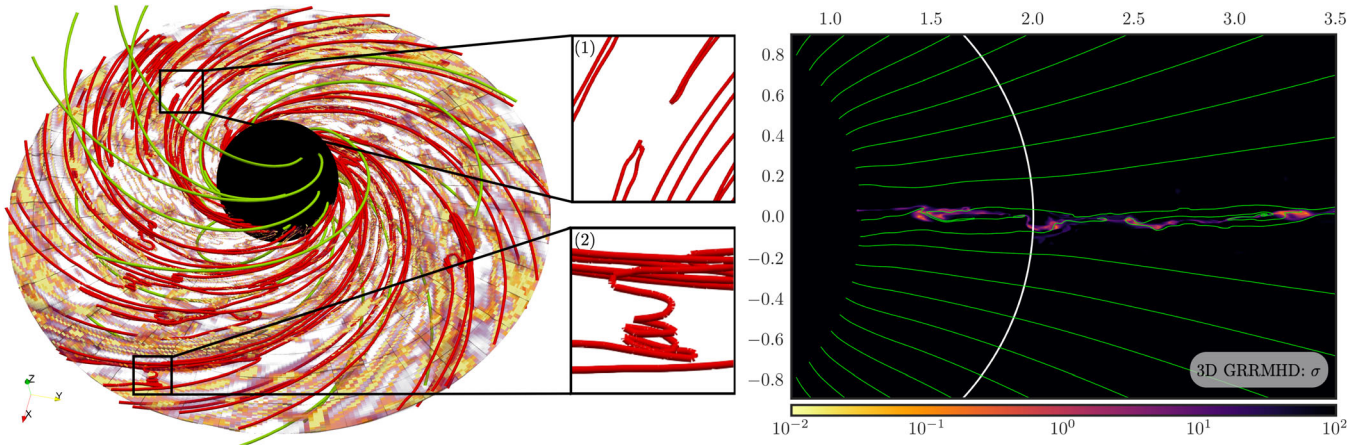
FIG. 4. Reconnecting magnetosphere in 3D (GRRMHD2) at $t = 118 \ r_g/c$. Left: volume rendering shows $\sigma = B^2/(4\pi\rho c^2)$, green tubes are magnetic field lines which penetrate the event horizon, red tubes are magnetic field lines which are reconnecting in the current sheet. Right: 2D slice of GRRMHD2 in the $\phi = 0$ half-plane. Color shows σ, green curves are magnetic field lines in the $\phi = 0$ half-plane. The picture highlights the nonaxisymmetric nature of reconnection in 3D, yet still displays similar fundamental structures— X points (inset 1), and helical winding of magnetic field lines in plasmoids (flux ropes) (inset 2).

reconnection rate observed by the FIDO is estimated by taking into account time dilation at the stagnation surface. For GRPIC1 it implies $\langle v^\theta \rangle/(c\alpha) \sim 0.05$, with α evaluated on the equator at the stagnation surface, consistent with the measured values.

In 3D (GRRMHD2), the balding proceeds similarly to the axisymmetric simulations (Fig. 3, cyan curve), but the plasmoid instability leads to nonaxisymmetric (in ϕ) structures. Therefore, 3D plasmoids, or flux tubes of tangled field lines with a finite extent in ϕ, generally display more complex topologies than those in 2D (Fig. 4).

The flux of conserved energy through spherical shells, as seen by an observer at infinity, is comparable in magnitude to $L_{\mathrm{BZ}} = 0.053\Omega_H^2\Phi^2/(4\pi c)$ [28], indicating successful activation of the Blandford-Znajek mechanism [6,23]. Large fluctuations up to several L_{BZ} are seen at the locations of plasmoids. We observe the emission of fast modes from plasmoid mergers (Fig. 2). In the high-σ limit, and where $B \sim 10^6$ G, these fast modes correspond to vacuum electromagnetic waves in the radio band, and could be observed as coherent radio emission [29]. The escaping giant plasmoids (Fig. 2) may shock the upstream wind, resulting in coherent synchrotron maser emission [30,31]. For collisionless plasma, we measure the total dissipative power as seen by an observer at infinity $L_{\mathrm{diss},\infty} \approx 0.4 L_{\mathrm{BZ}}$. When the magnetic field is strong ($B \gtrsim 10^6$ G) as expected in BH-NS mergers, the reconnection is radiative and most of the dissipated magnetic energy will go into photons. In this regime, $L_{\mathrm{diss},\infty} \approx 0.4 L_{\mathrm{BZ}} \sim 4 \times 10^{45} M_{10\odot}^2 B_{12}^2$ erg s^{-1} corresponds to emission in the hard x-ray band [32]. We also observe a population of negative energy-at-infinity particles localized in the current sheet inside the ergosphere. They contribute to $\boldsymbol{J} = (c/4\pi)\nabla \times \boldsymbol{H}$, and some are advected into the BH with plasmoids—an instance of the Penrose process facilitated by magnetic reconnection [7,33].

We considered Kerr BH's endowed with highly magnetized plasma-filled magnetospheres. We find that (i) the no-hair theorem holds, in the sense that all components of the stress-energy tensor decay exponentially in time; (ii) reconnection occurs at the universal rate when measured in the locally Minkowski frame of the FIDO; (iii) the lifetime of the magnetic field on the event horizon is controlled by the local reconnection rate measured by the FIDO in concert with other global effects; and (iv) the final state is a Kerr BH with charge $Q = 0$. Balding BHs resulting from the merger or collapse of compact objects should appear as a spectacular source of hard x-ray emission for a short duration, similar to the flares of galactic magnetars. Observation of the x-ray emission requires a clean environment around the BH. It is possible during the gravitational collapse of a rotationally supported massive neutron star, and in BH-NS mergers with a high mass ratio, so that the NS falls through the event horizon without forming a torus or disk. Gamma-ray bursts and other collapsars may be different to the scenario described in this work, depending on how much matter surrounds the newly formed BH. The decay of magnetic flux on the event horizon may also explain powerful x-ray and near-infrared flares and hot spots [34] driven by plasmoid-regulated reconnection in magnetically dominated supermassive BH magnetospheres [19,33]. The faster reconnection rate in collisionless plasma implies that larger plasmoids, powering a flare near the BH, can form in a shorter time and in this way regulate the typical flare duration.

———

[*]ashley.bransgrove@columbia.edu

[1] H. Falcke and L. Rezzolla, Astron. Astrophys. **562**, A137 (2014).

[2] I. Goldman and S. Nussinov, Phys. Rev. D **40**, 3221 (1989).

[3] W. E. East, L. Lehner, S. L. Liebling, and C. Palenzuela, Astrophys. J. Lett. **912**, L18 (2021).

[4] C. W. Misner, K. S. Thorne, and J. A. Wheeler, *Gravitation* (W. H. Freeman and Company, San Francisco, 1973).

[5] R. H. Price, Phys. Rev. D **5**, 2439 (1972).

[6] R. D. Blandford and R. L. Znajek, Mon. Not. R. Astron. Soc. **179**, 433 (1977).

[7] K. Parfrey, A. Philippov, and B. Cerutti, Phys. Rev. Lett. **122**, 035101 (2019).

[8] B. Crinquand, B. Cerutti, A. Philippov, K. Parfrey, and G. Dubus, Phys. Rev. Lett. **124**, 145101 (2020).

[9] M. Lyutikov and J. C. McKinney, Phys. Rev. D **84**, 084019 (2011).

[10] A. Bhattacharjee, Y.-M. Huang, H. Yang, and B. Rogers, Phys. Plasmas **16**, 112102 (2009).

[11] L. Sironi and A. Spitkovsky, Astrophys. J. Lett. **783**, L21 (2014).

[12] F. Guo, H. Li, W. Daughton, and Y.-H. Liu, Phys. Rev. Lett. **113**, 155005 (2014).

[13] G. R. Werner, D. A. Uzdensky, B. Cerutti, K. Nalewajko, and M. C. Begelman, Astrophys. J. **816**, L8 (2015).

[14] L. Lehner, C. Palenzuela, S. L. Liebling, C. Thompson, and C. Hanna, Phys. Rev. D **86**, 104035 (2012).

[15] P. Goldreich and W. H. Julian, Astrophys. J. **157**, 869 (1969).

[16] O. Porth, H. Olivares, Y. Mizuno, Z. Younsi, L. Rezzolla, M. Moscibrodzka, H. Falcke, and M. Kramer, Comput. Astrophys. Cosmol. **4**, 1 (2017).

[17] H. Olivares, O. Porth, J. Davelaar, E. R. Most, C. M. Fromm, Y. Mizuno, Z. Younsi, and L. Rezzolla, Astron. Astrophys. **629**, A61 (2019).

[18] B. Ripperda, F. Bacchini, O. Porth, E. R. Most, H. Olivares, A. Nathanail, L. Rezzolla, J. Teunissen, and R. Keppens, Astrophys. J. Suppl. Ser. **244**, 10 (2019).

[19] B. Ripperda, F. Bacchini, and A. A. Philippov, Astrophys. J. **900**, 100 (2020).

[20] B. Ripperda, O. Porth, L. Sironi, and R. Keppens, Mon. Not. R. Astron. Soc. **485**, 299 (2019).

[21] N. Bessho and A. Bhattacharjee, Phys. Rev. Lett. **95**, 245001 (2005).

[22] D. A. Uzdensky, N. F. Loureiro, and A. A. Schekochihin, Phys. Rev. Lett. **105**, 235002 (2010).

[23] See Supplemental Material at http://link.aps.org/supplemental/10.1103/PhysRevLett.127.055101 for descriptions of the numerical convergence, collisionality, decay timescale, and luminosity, which includes Refs. [24–26].

[24] D. A. Uzdensky, Space Sci. Rev. **160**, 45 (2011).

[25] F. C. Michel, Astrophys. J. Lett. **180**, L133 (1973).

[26] A. Tchekhovskoy, A. Philippov, and A. Spitkovsky, Mon. Not. R. Astron. Soc. **457**, 3384 (2016).

[27] B. Crinquand, B. Cerutti, G. Dubus, K. Parfrey, and A. Philippov, arXiv:2012.09733.

[28] A. Tchekhovskoy, R. Narayan, and J. C. McKinney, Mon. Not. R. Astron. Soc.: Lett. **418**, L79 (2011).

[29] A. Philippov, D. A. Uzdensky, A. Spitkovsky, and B. Cerutti, Astrophys. J. **876**, L6 (2019).

[30] Y. Lyubarsky, Mon. Not. R. Astron. Soc. **442**, L9 (2014).

[31] A. M. Beloborodov, Astrophys. J. **843**, L26 (2017).

[32] A. M. Beloborodov, arXiv:2011.07310.

[33] L. Comisso and F. A. Asenjo, Phys. Rev. D **103**, 023014 (2021).

[34] R. Abuter *et al.* (Gravity Collaboration), Astron. Astrophys. **618**, L10 (2018).